

Distinct modes of East Asian Winter Monsoon documented by a southern Red Sea coral record

Monica Ionita (1,2), Thomas Felis (2), Gerrit Lohmann (1,2), Norel Rimbu (1,3), Jürgen Pätzold (2)

1. Alfred Wegener Institute Helmholtz Center for Polar and Marine Research, 27570 Bremerhaven, Germany
2. MARUM – Center for Marine Environmental Sciences, University of Bremen, 28359 Bremen, Germany
3. Climed Norad, Bucharest, Romania

Corresponding author:

Email: Monica.Ionita@awi.de

Address: Alfred Wegener Institute Helmholtz Center for Polar and Marine Research

Bussestrasse 24

D-27570 Bremerhaven

Telephone: +49(471)4831-1845

Fax: +49(471)4831-1271

This article has been accepted for publication and undergone full peer review but has not been through the copyediting, typesetting, pagination and proofreading process which may lead to differences between this version and the Version of Record. Please cite this article as doi: 10.1002/2013JC009203

© 2014 American Geophysical Union

Received: Jun 13, 2013; Revised: Dec 09, 2013; Accepted: Jan 19, 2014

Abstract

The large-scale boreal winter climatic patterns associated with interannual variability in a coral oxygen isotope ($\delta^{18}\text{O}$) record from the southern Red Sea (Klein et al. [1997]) covering most of the last century are investigated. From the early 1930's to the early 1960's, the winter coral $\delta^{18}\text{O}$ record, reflecting temperature and salinity variations in southern Red Sea surface waters, is associated with global (or large scale) sea surface temperature (SST) and 850mb geopotential height (Z850) anomalies which project on the corresponding patterns associated with the El Niño-Southern Oscillation (ENSO). In contrast, since the early 1960's the winter coral $\delta^{18}\text{O}$ record is related to a Z850 pattern that reflects the ENSO-independent part of the East Asian Winter Monsoon (EAWM), which includes the Siberian High, the East Asian through and the East Asian upper-tropospheric Jet. Our results indicate a weakening of the ENSO control on interannual temperature/salinity variations in southern Red Sea surface waters in the early 1960's, due to the warming of the Indian Ocean, and suggest that information about the non-stationarity in the relationship between ENSO and two distinct modes of EAWM can be documented in southern Red Sea coral $\delta^{18}\text{O}$ records.

Key words: ENSO, East Asian Winter Monsoon, Red Sea, Coral

1. Introduction

[1] The understanding of the cause of climate changes requires extensive data sets. Where observational data are missing or the coverage is sparse, proxy data derived from paleoclimatic archives can be used to obtain climatic information. Furthermore, proxy records document climate variations back in time before the instrumental period. Massive, annually-banded corals represent an extensively used proxy data source, which provides annually to monthly resolved records from the tropical and subtropical oceans. Important coral proxies for sea surface temperature (SST) include $\delta^{18}\text{O}$ (e.g., Charles et al., 1997; Cole et al., 2000; Felis et al., 2000) and Sr/Ca (Beck et al., 1992; Linsley et al., 2000; Felis et al., 2004; Pfeiffer et al., 2006). The variability of these coral-based proxies ($\delta^{18}\text{O}$, Sr/Ca) is not only used to reconstruct local climatic variability, but also large-scale phenomena like the El Niño-Southern Oscillation (ENSO) (Cole et al., 1993; Cobb et al., 2003), Arctic/North Atlantic Oscillation (AO/NAO) (Felis et al., 2000; Rimbu et al., 2001; Felis and Rimbu, 2010) or the Pacific Decadal Oscillation (Felis et al., 2010). Coral records from the Indian Ocean have been shown to adequately resolve the ENSO and monsoon interactions as expressed in SST variations (Charles et al., 1997; 2003; Cole et al., 2000, Zinke et al., 2005; Pfeiffer and Dullo, 2006).

[2] ENSO is a coupled ocean-atmosphere phenomenon that is the most dominant source of interannual climate variability. It originates in the tropical Pacific and generates extreme weather events such as droughts, floods, and tropical cyclones, across vast regions of the globe (Chan, 1985; Power et al., 1999). Although its impact on climate has been extensively studied, many characteristics of the long-term changes in ENSO frequency, magnitude and duration are not fully understood. The interaction between ENSO and climate variability in the Indian Ocean has been the subject of many studies (Cadet, 1985; Kug and Kang, 2006; Zhong et al., 2005). In general, positive (negative) sea surface temperature (SST) anomalies

in the western and central Indian Ocean are associated with warm (cold) ENSO anomalies. To a large extent the ENSO – Indian Ocean climate relationship is controlled by the Walker circulation (Lau and Nath, 2000, 2003; Krishnamurthy and Kirtman, 2003). The changes in the atmospheric circulation which accompany ENSO were shown to induce changes in the Indian Ocean SST via changes in the evaporation and cloud cover (Klein et al., 1999). However, it has been shown that variability of the Indian Ocean can also modulate ENSO (e.g. Saji and Yagamata, 2003; Annamalai et al., 2005; Kug and Kang, 2006). According to Kug and Kang (2006) the warming in the Indian Ocean during an ENSO warm event produces an easterly wind stress anomaly over Indonesia and the western Pacific, which in turn produces a rapid termination of the ENSO warm event (El Niño) and a fast transition towards an ENSO cold event (La Niña).

[3] A phenomenon different from ENSO is the Asian winter monsoon. The East Asian Winter Monsoon (EAWM) is the main mid-latitude part of the Asian winter monsoon. EAWM is one of the most active systems in Northern Hemisphere winter and exerts strong impacts on the large-scale atmospheric circulation in the tropics and extratropics (Chang and Lau, 1982) and even influences the convection and SST near the maritime continent (Chang et al. 2006). The EAWM dominates a large area of East Asia with persistent influence in boreal winter and it comprises the Siberian High, the East Asian trough and the East Asian jet stream, which are located in the lower, mid and upper troposphere, respectively. At the surface, EAWM is characterized by the cold core of the Siberian High, the Aleutian Low, a large surface temperature gradient over East Asia and predominant north-easterly winds from the western North Pacific to the Arabian Sea (Wang, 2006). The EAWM is associated with cold surges and heavy snowfall events over East Asia (Boyle and Chen, 1987; Wei et al., 2011; Li and Wang, 2012) and rainfall over southeastern and southern China (Zhou, 2011).

[4] ENSO and EAWM interact with each other on interannual and decadal time scales. This interaction is thought to be an important factor controlling the EAWM (Wang, 2006). For example, El Niño (La Niña) events result in a weaker (stronger) winter monsoon (Zhang et al., 1996). EAWM is usually seen as a singular system, but recent studies show that EAWM is characterized by distinct modes (Wu et al., 2006). Wu et al. (2006) showed that EAWM is characterized by two distinct modes: a) an EAWM mode independent of ENSO and b) an EAWM mode dependent of ENSO. The first mode is strongly related to the Siberian High, the East Asian trough and the East Asian upper-tropospheric jet, while the second one is closely related to atmospheric features that project onto ENSO related anomalies. Gong et al. (2001) showed that another factor that influences the EAWM on interannual timescales is the AO. They pointed out that AO influences EAWM through impacts on the winter Siberian High. However, Wu and Wang (2002) showed that AO and Siberian High are independent of each other in influencing EAWM, and suggested that the main influence of AO on EAWM is via the surface air temperature, sea level pressure (SLP) and the East Asian trough, rather than via the Siberian High.

[5] Using a coral $\delta^{18}\text{O}$ record from the northern Red Sea (Felis et al., 2000), Rimbu et al. (2003) showed that the relationship between ENSO and the climate over Europe and the Middle East has varied since the beginning of the instrumental era. The coral record from the northern Red Sea is mainly linked to the AO (Rimbu et al., 2001; Felis et al., 2004; Felis and Rimbu 2010), which is the dominant mode of atmospheric variability over the Northern Hemisphere during winter. On the other hand, Klein et al. (1997) using a coral record from the southern Red Sea showed that this record can be a good indicator of the NE monsoon and ENSO variability, but no connection with the extratropical circulation has been shown. Importantly, the processes that are driving the coral $\delta^{18}\text{O}$ variability, in the northern and southern Red Sea, are very different, an aspect which was emphasized also by Felis et al.

(2000). In a recent paper, Papadopoulos et al. (2013) showed that the air-sea heat fluxes over the Red Sea are associated with an atmospheric circulation pattern that enhances the advection of cold and dry air from the mid-latitudes towards the Red Sea. They found that this SLP pattern is not directly related with one of the main leading modes of variability (e.g., NAO or AO).

[6] In this study we analyze the relation between the Dahlak coral $\delta^{18}\text{O}$ record from the southern Red Sea (Klein et al., 1997) and ENSO and EAWM variability, and investigate possible links of this record with the extratropical climate variability. We also study whether the relationship between ENSO, EAWM and the coral $\delta^{18}\text{O}$ record can be regarded as stationary, i.e., is not changing in time. There are indications that the relationship between ENSO and the climate teleconnection patterns is not stationary. Timm et al. (2005) found evidence of a non-stationary relationship between ENSO and a coral $\delta^{18}\text{O}$ record from the central Indian Ocean. Recently, Nakamura et al. (2009) found new evidences of a mode shift in the Indian Ocean at the beginning of the 1960's. They argue that around this time there was a shift from an ENSO-monsoon mode to an Indian Ocean Dipole (IOD) - monsoon mode.

[7] Although the relationship between the southern Red Sea coral record and large-scale atmospheric and oceanic circulation patterns, including the ENSO teleconnection, has been investigated (Klein et al., 1997) no conclusions regarding the stability of the coral $\delta^{18}\text{O}$ – ENSO relationship and possible mechanisms controlling a potential non-stationarity were drawn at that time. Moreover, Klein et al. (1997) reported that the coral record is an indicator of the NE monsoon, but no actual comparison to an index of the NE monsoon has been made. In our study we show, based on a systematic comparison of the coral $\delta^{18}\text{O}$ record with an EAWM index, that the Dahlak coral $\delta^{18}\text{O}$ record from the southern Red Sea (Klein et al., 1997) captures two distinct modes of the EAWM and that the influence of these two modes

on the variability of the coral record is sensitive to the observed Indian Ocean warming of the last 50 years. Although Klein et al (1997) focused their analysis on the NE Monsoon, we choose to focus on the EAWM for two main reasons: a) EAWM is an integrated part of the Asian winter monsoon (Wang, 2006) and can be easily quantified with a number of indices (Hui, 2007), and b) EAWM is strongly related to the extratropical atmospheric circulation (e.g. Siberian High, East Asian Jet), a connection that has not been investigated by Klein et al. (1997). In this manuscript we will show that the extratropical atmospheric circulation, modulated by the EAWM, plays an important role in southern Red Sea coral $\delta^{18}\text{O}$ variability. To our knowledge, the influence of distinct modes of the EAWM and their relationship with ENSO has not been studied using a high-resolution coral archive of surface ocean conditions.

The paper is structured as follows: in section 2 the description of the study area and the used data sets are made. Section 3 presents the results. An extended discussion is included in section 4. The conclusions are presented in section 5.

2. Data and methods

[8] The Red Sea is a body of very saline water which is located between Africa and Asia. The connection to the Indian Ocean in the South is through the Bab el Mandeb Strait and the Gulf of Aden. During the winter monsoon season, southerly winds dominate the southern Red Sea region (Figure 1). North of about 18° N, where a strong convergence zone is located, northwesterly winds are prominent during this season. This convergence zone marks the boundary between the monsoon dominated atmosphere of the southern Red Sea and that of the northern Red Sea which is influenced by continental climate. Most of the Red Sea is located in the sub-tropical high belt and is influenced by subsidence of the Hadley cell. Salinity ranges from ~ 36 (ppt) in the southern part due to the effect of the Gulf of Aden water

and reaches 41 (ppt) in the northern part, mainly due to the high evaporation. The average salinity is 40 (ppt). The mean SST in January-February ranges from about 20 °C in the far north to about 27 °C in the south.

[9] In this study we investigate a coral $\delta^{18}\text{O}$ record from the southern Red Sea, originally published by Klein et al. (1997). The bimonthly resolved record covers the period 1931-1992. It was generated from a *Porites* colony drilled at Dur-Ghella Island (core DGII) in the Dahlak Archipelago of the southern Red Sea (15° 43' N; 39° 54' E), off the coast of Eritrea. The $\delta^{18}\text{O}$ signal incorporated into coral skeletons during growth is influenced by both the temperature and the $\delta^{18}\text{O}$ of the ambient seawater (Eshel et al., 2000; Felis et al., 2000; Klein et al., 1997). Positive coral $\delta^{18}\text{O}$ anomalies reflect lower SST and more saline conditions, and vice versa for negative coral $\delta^{18}\text{O}$ anomalies. In this study we concentrate on boreal winter (January-February (JF)) coral $\delta^{18}\text{O}$, thus JF means were extracted from the bimonthly coral record. The resulting time series was linearly detrended and normalized by its standard deviation.

[10] The temperature over land (TT), for the period 1931-1992, was taken from the CRU (Climatic Research Unit) TS3.20 data set (Harris et al., 2013), which has a 0.5° x 0.5° resolution. The global SST data, for the period 1931-1992, was extracted from the Hadley Centre Sea Ice and Sea Surface Temperature data set (HadISST2, Rayner et al., 2003). This data set covers the period 1871 – 2012 and has a 1° x 1° resolution. For the Northern Hemisphere atmospheric circulation we use the geopotential height at 850mb (Z850), zonal wind at 850mb (u850) and the meridional wind at 850mb (V850) on a 2° x 2° grid from Twentieth Century Reanalysis (V2) data (Compo et al., 2006, 2011; Whitaker et al., 2004), for the period 1931-1992. From the same data sets we have extracted the wind components at the 200mb level in order to compute the velocity potential and the divergent wind.

[11] All instrumental data sets were processed in the same way. First, the winter (November-December-January-February (NDJF)) means for (TT, SST, Z850, U850 and V850) were calculated from the monthly means. Then, seasonal anomalies with respect to the mean and normalized by standard deviation, estimated for the period 1931-1992, were produced.

[12] The EAWM intensity was estimated with a winter (NDJF) index, which is defined as the area-averaged SLP anomaly difference between (110–120° E, 20–45° N) and (150–160° E, 20–45° N) (Zhou et al., 2007). Positive (negative) values of this index indicate a strong (weak) EAWM. The EAWM index was separated into two components: an ENSO dependent and an ENSO independent component. The ENSO related component was calculated by linear regression of the EAWM index with respect to the winter Niño 3.4 index, and is termed $EAWM_{en}$. The winter (NDJF) Niño 3.4 index is defined as the area averaged SST (HadISST2, Rayner et al., 2003) anomalies in the region of 170° W - 120° W and 5° S - 5° N. The ENSO independent component of the EAWM, which is termed $EAWM_{res}$, was computed as the difference between the EAWM index and its ENSO dependent component ($EAWM_{en}$). The winter (NDJF) Siberian High index was computed by averaging SLP over the key region between 40°–65° N and 80°–120° E (Panagiotopoulos et al., 2005).

3. Results

3.1 Time series analysis

[13] The time series of the Dahlak coral $\delta^{18}O$ record for JF along with the Niño 3.4 index for NDJF are shown in Figure 2. The correlation coefficient between the two time series over the whole analyzed period (1931-1992) is $r = -0.30$ (95% significance level). However, for the period 1931 – 1961 the correlation coefficient is $r = -0.63$, while for the period 1962 – 1992 it becomes almost zero ($r = -0.08$). Motivated by the difference in the correlation coefficient

between coral $\delta^{18}\text{O}$ record and Niño 3.4 index, we address the question of non-stationarity in the relationship between the coral record and ENSO, and investigate the potential role of the EAWM and Siberian High in this non-stationarity.

[14] In order to test the strength of the relationship between the Dahlak coral $\delta^{18}\text{O}$ record and the Niño 3.4, Siberian High and EAWM indices (EAWM_{en} and EAWM_{res}) we calculate the corresponding correlation coefficients for a 21-year moving window. Prior to the correlation analysis the time series were linearly detrended and normalized by their standard deviation. In Figure 3a we show the running correlations in a 21-year moving window between the winter coral record and Niño 3.4, winter EAWM index and winter EAWM_{en} index. The correlation coefficients reveal a non-stationary behavior in the correlation between the coral $\delta^{18}\text{O}$ time series and the teleconnection indices on interannual time scales. A strong negative (positive) correlation is found between coral $\delta^{18}\text{O}$ and Niño 3.4 (EAWM_{en}) for the period prior to the 1960's. After the beginning of the 1960's, the strength of the correlation decays abruptly, and a strong negative correlation is then found between the coral $\delta^{18}\text{O}$ record and EAWM index. In Figure 3b we show the running correlations in a 21-year moving window between the winter coral record and winter EAWM_{res} index (red dotted line) and winter Siberian High (SIB) index (blue dotted line). Contrasting to Figure 3a, the correlation coefficients between the aforementioned time series are significant after the beginning of 1960's.

[15] To further test the question of non-stationarity of the climate signal in the Dahlak coral $\delta^{18}\text{O}$ time series, we performed a Morlet wavelet analysis (Torrence and Compo, 1998; Grinsted et al., 2004) of coral time series and Niño3.4 index. By decomposing the time series into time-frequencies space, we are able to determine both the dominant modes of variability and their evolution in time. The Morlet wavelet spectrum (Figure 3c) of the linear detrended and normalized coral $\delta^{18}\text{O}$ time series shows a nonstationary behavior for the ENSO band,

which emphasizes the fact that the strength of this variability in the coral $\delta^{18}\text{O}$ time series has varied in time. Furthermore, the coherence between the coral $\delta^{18}\text{O}$ time series and Niño 3.4 has also varied in time (Figure 3d). The greatest coherency occurs in the 4 to 8 year band, during the period between 1935 and 1960. From 1960 to 1975 the relationship between coral $\delta^{18}\text{O}$ and Niño 3.4 is very weak. Starting in the 1960's there is some coherency between coral $\delta^{18}\text{O}$ and Niño 3.4 in the 10 to 16 years band.

3.2 Winter coral $\delta^{18}\text{O}$ variability and large-scale climate patterns

[16] In order to study the SST, TT and atmospheric circulation patterns associated with the interannual variability in the Dahlak coral $\delta^{18}\text{O}$ record during winter, before and after the 1960's shift, as identified in the previous section, we constructed the correlation (composite) maps between the coral record and SST, TT (geopotential height at 850mb, wind vectors at 850mb and velocity potential at 200 b) for two distinct periods: 1931 – 1961 and 1962 – 1992, respectively. For a better comparison with the monsoon index we make the same analysis for the EAWM_{en} and EAWM_{res} indices. Taking into account the results from Figure 3a and b, we will show also the correlation (composite) maps between winter EAWM_{en} index and winter global SST (geopotential height at 850mb and wind vectors at 850mb) for the period 1931 – 1961 (for this period the coral record is significantly correlated with the winter EAWM_{en} index) and the correlation (composite) maps between winter EAWM_{res} index and winter global SST (geopotential height at 850mb and wind vectors at 850mb) for the period 1962 – 1992 (for this period the coral record is significantly correlated with the winter EAWM_{res} index).

[17] The composite maps are defined by average fields of Z850, meridional and zonal wind at 850mb level and velocity potential for winters when coral $\delta^{18}\text{O}$, the winter EAWM_{en} index and the winter EAWM_{res} index was higher (lower) than 0.75 (-0.75) standard deviation. This

threshold was chosen as a compromise between the strength of the climate anomalies associated with coral $\delta^{18}\text{O}$ anomalies and the number of maps which satisfy this criterion. Further analysis showed that the results are not sensitive to the exact threshold value used for composite analysis (not shown). The level of significance of the composite maps is established by means of a Student's t test (e.g., von Storch and Zwiers, 1999).

3.2.1 Relationship with global SST

[18] The correlation maps with winter global SST show that the interannual variability of Dahlak coral $\delta^{18}\text{O}$ during winter is controlled by distinct SST patterns in the two analyzed periods. Consistent with the wavelet power spectrum (Figure 3d), positive coral $\delta^{18}\text{O}$ anomalies are associated with a typical La Niña-SST pattern during 1931 - 1961 (Figure 4a), with negative SST anomalies in the eastern tropical Pacific and the northwestern Indian Ocean, and positive SST anomalies in the far western tropical Pacific. The SST anomalies emphasize the strong link between the Pacific and Indian Ocean in driving large-scale climate variability. It is difficult to estimate which of the two oceans plays the most important role in the variability of the winter Dahlak coral $\delta^{18}\text{O}$ time series, since SST anomalies in the Indian Ocean coevolve with those in Pacific. Figure 4b shows the correlation map between the winters EAWM_{en} index and winter global SST. As in the case of the coral record, the SST pattern projects onto the SST anomalies associated with La Niña conditions. Figure 4b is almost identical with Figure 4a, implying that for the period 1931 – 1961 both ENSO and EAWM_{en} have a strong impact on the winter coral record variability, in agreement with Figure 3a. La Niña conditions associated with a strong EAWM_{en} trigger positive coral $\delta^{18}\text{O}$ anomalies in the southern Red Sea.

[19] The correlation maps between the winter coral record and winter EAWM_{res} index, with winter global SST for the period 1962 – 1992 (Figure 4c and 4d) show completely distinct

features than the maps for the period 1931-1961. Positive Dahlak coral $\delta^{18}\text{O}$ anomalies during winter are associated with negative SST anomalies in the eastern Mediterranean Sea and with SST anomalies in the North Atlantic Ocean that show similarities to the SST pattern associated with the positive phase of the North Atlantic Oscillation (NAO). Positive coral $\delta^{18}\text{O}$ anomalies are also associated with negative SST anomalies in regions of the high- and low-latitude Pacific Ocean (Figure 4c). A similar pattern we obtain when we compute the correlation map between the winter EAWM_{res} index and winter global SST (Figure 4d), for the period 1962 – 1992. Based on Figure 4d a weak EAWM_{res} is associated with a limb of positive SST anomalies in the north-western Pacific Ocean flanked by positive SST anomalies and a tripole-like SST anomalies in the Atlantic Ocean similar to the one in Figure 4c. The main difference between Figure 4c and Figure 4d is the sign of the correlation over the central Indian Ocean.

3.2.2 Relationship with geopotential height and wind at 850mb

[20] For the geopotential height and wind at 850mb composite maps the differences for the two analyzed periods are evident as well (Figure 5a-c and Figure 6a-c, respectively). For the period 1931 – 1961 positive $\delta^{18}\text{O}$ anomalies are associated with significant negative Z850 anomalies over the entire tropical Atlantic Ocean, the whole Indian Ocean and the tropical western Pacific Ocean, while positive anomalies appear over the whole Eurasian continent and the North Pacific (Figure 5a). In order to better assess the Z850 anomaly patterns that influence the coral $\delta^{18}\text{O}$ anomalies we construct the composite maps of 850mb wind with the winter coral record (Figure 5a and 5c (vectors)) and EAWM_{en} index (Figure 5b) for the period 1931 – 1961. In agreement with the atmospheric circulation at the 850mb level, positive $\delta^{18}\text{O}$ anomalies are associated with the advection of cold SST anomalies from the northern Indian Ocean (see the black arrow in Figure 5c). The same wind related anomalies are obtained when we compute the composite map between EAWM_{en} index and wind at

850mb, for the period 1931 – 1961. This is additional evidence that for the period 1931 – 1961 positive coral $\delta^{18}\text{O}$ anomalies are influenced by ENSO related anomalies, via the advection of cold SST from the Indian Ocean. A similar pattern to the one in Figures 5a – b, but for the geopotential height at the 500mb level, was identified by Wu et al. (2006) showing that these anomalies are related to a phase of the EAWM which is dependent of ENSO.

[21] In contrast, the composite map between the winter coral record and the geopotential height and wind at the 850mb level, for the period 1962 – 1992, is characterized by negative anomalies over northeastern Asia and western North America with concurrent positive anomalies over the North Pacific, the whole African continent and southern Europe and eastern North America (Figure 6a). This kind of atmospheric circulation allows the advection of cold and dry air from the southern part of Europe and the northern Red Sea towards the central and southern Red Sea (see the black arrow in Figures 6c). These Z850 anomalies are related to a phase of the EAWM which is independent of El Niño (Wu et al., 2006) and more related to the variability of the Siberian High and the East-Asian upper tropospheric jet. The composite map between the winter EAWM_{res} index and the geopotential height and wind at the 850mb level (Figure 6b), for the period 1962 – 1992, resembles Figure 6a, but in the case of the EAWM_{res} index the centers of the negative (positive) anomalies over northeastern Asia (the central Pacific) are much stronger. Based on Figure 6a and 6b, we can conclude that positive $\delta^{18}\text{O}$ anomalies are associated with a weak EAWM_{res} , a weak Siberian High (the negative Z850 anomalies over the northern part of Eurasia) and a weak East Asian jet, which allow perturbations from the North Atlantic and the Mediterranean Sea to penetrate towards the Eurasian continent, in this way creating a steep Z850 gradient over the Arabian Peninsula which allows the advections of cold and dry air from the north towards the Red Sea. When the ENSO signal is removed, during the positive AO/NAO winters an anomalous Rossby wave activity develops which propagates to the northern Arabian Sea and brings anomalous

northern winds over the Red Sea and the northern Indian Ocean (Gong et al., 2013). This result is in agreement with our findings that when ENSO signal is blocked and does not reach the Indian Ocean, the North Atlantic atmospheric circulation can have an influence until the northern Indian Ocean including the Red Sea.

3.2.3 Relationship with temperature (TT) over land

[22] The winter Dahlak coral $\delta^{18}\text{O}$ record is strongly related with winter temperature over land (Figure 7a and 7b, respectively). The TT patterns are dynamically consistent with the SST (Figure 4a and 4c) and Z850 patterns (Figure 5a and Figure 6a). For the period 1931 – 1961, positive coral $\delta^{18}\text{O}$ anomalies are associated with negative TT anomalies over southern Asia, the southernmost Arabian Peninsula and the Horn of Africa and with positive TT anomalies over Europe and northern Africa (Figure 7a). This spatial pattern resembles the temperature anomalies over land associated with the cold phase of ENSO (Marengo, 1992; Ronchail et al., 2002).

[23] For the period 1962 - 1992, positive coral $\delta^{18}\text{O}$ anomalies are associated with weak negative TT anomalies over North Africa, Arabian Peninsula and Siberia and with positive TT anomalies over Europe and central to eastern Asia (Figure 7b). The cold temperatures over North Africa and the Arabian Peninsula are advected towards the southern Red Sea and contribute to the positive $\delta^{18}\text{O}$ anomalies, in agreement with Figure 5c. Similar results (not shown) are obtained when we compute the correlation maps between winter EAWM_{en} index and winter TT for the period 1931 – 1961 (similar to Figure 7a) and winter EAWM_{res} index and winter TT for the period 1962 – 1992 (similar to Figure 7b).

4. Discussion

[24] In this study we investigate the large-scale teleconnections associated with the interannual variability of a southern Red Sea coral $\delta^{18}\text{O}$ record during boreal winter, originally presented by Klein et al. (1997). We found that the connection between the winter Dahlak coral $\delta^{18}\text{O}$ record and ENSO and EAWM is non-stationary over the last century and the coral record variability is influenced by two distinct modes of the EAWM over the two different periods: 1931 – 1961 and 1962 – 1992, respectively. The running correlation between the coral record and the winter Niño 3.4 index and the winter EAWM_{en} index indicates an abrupt change in the early 1960's, from significantly negative (positive) since the early 1930's to non-significantly positive (negative) (Figure 3a). In the same time, the running correlation between the coral record and the winter EAWM_{res} becomes significantly negative after the beginning of the 1960's (Figure 3b). In order to reveal the physical processes responsible for this change in the relationship to ENSO and EAWM, we study the corresponding changes in large-scale atmospheric circulation and sea surface temperature during the period before and after the shift, respectively.

[25] Comparable results of a non-stationary relationship with ENSO throughout the last century were reported from other sites in the Indian Ocean. Timm et al. (2005) demonstrated that a strong relationship between ENSO and their coral $\delta^{18}\text{O}$ record from the central Indian Ocean only emerged after the mid-1970's. This finding is consistent with a climate regime shift in the mid-1970's that has been extensively documented throughout the Pacific Ocean (e.g., Trenberth and Hurrell, 1994; Zhang et al., 1997, Rimbu et al., 2003). On the other hand, using a coral record from Kenya, Nakamura et al. (2009) showed a mode shift in the Indian Ocean climate through the 20th century. Their study suggested that since 1960's the frequent and intensified Indian Ocean Dipole (IOD) events, due to the Indian Ocean warming, dominated the tropical Indian Ocean climate and overshadowed the ENSO – Indian Ocean

Summer Monsoon interaction. The shift in the 1960's identified by Nakamura et al. (2009) is in agreement with our results regarding the non-stationary relationship between the southern Red Sea coral and ENSO and EAWM and the abrupt shift of this relationship at the beginning of the 1960's.

[26] The climate maps related to the winter Dahlak coral $\delta^{18}\text{O}$ indicate that the 1931 – 1961 period is characterized by climate anomalies reminiscent of ENSO features, while the 1962 – 1992 period is characterized by climate anomalies and a phase of the winter monsoon which is independent of ENSO but closely related to the variability of the Siberian High and the East – Asian Jet (Figure 5 and 6). We speculate that the observed changes could be induced by the global warming trend in SST, especially the positive SST trend in the Indian Ocean, which can act as a barrier for the ENSO influence on the Indian Ocean and surrounding areas (Nakamura et al., 2009). Since ~1950 there is evidence for a weakening of the SLP gradient between the western Pacific – Indonesian region and the eastern tropical Pacific. This suggests a weakening of the Walker circulation (Zhang and Song, 2006), which could act as a barrier for the ENSO influence on the Indian Ocean region. A modeling study suggests that even a modest warming of the Indian Ocean can act as a significant factor in suppressing the convection over the maritime continent (Watanabe and Jin, 2002). In their baroclinic model they showed that the Indian Ocean warming will modify the Walker circulation which in return will weaken the convection over the western Pacific.

[27] To support this idea we have plotted the composite maps between the winter Dahlak coral $\delta^{18}\text{O}$ record and the 200mb velocity potential and the divergent wind. The different SST composite maps for the two analyzed periods correspond to different zonal atmospheric circulation anomalies. For the first period analyzed (1931 – 1961) high coral $\delta^{18}\text{O}$ anomalies are associated with a well organized zonal tripole structure over the tropical Pacific Ocean and the tropical Indian Ocean (Figure 8a). A region of divergence over the western tropical

Pacific and the maritime continent is flanked by two regions of convergence over the western tropical Indian Ocean and the central tropical Pacific Ocean. The convergence over the central Pacific is stronger than that over the western Indian Ocean, implying that the ascending motion over the western Pacific is more linked to the descending motion over the central-eastern Pacific compared to that over the western Indian Ocean. This pattern is reminiscent of the Walker circulation that prevails during La Niña conditions, which is in agreement with the corresponding SST composite map (Figure 3a) for the period 1931 – 1961 (positive $\delta^{18}\text{O}$ anomalies are associated with La Niña like SST anomalies).

[28] Changes in atmospheric convection are a clue for a Walker circulation slowdown.

Tokenaga et al. (2012) demonstrated that there has been an eastward shift of precipitation and cloudiness from the maritime continent to the central Pacific, accompanied by changes in the surface wind convergence, in the last 60 years. Interestingly, our analysis reveals that high coral $\delta^{18}\text{O}$ anomalies during the period 1962 – 1992 are associated with a region of convergence that covers most of the Indian Ocean, the maritime continent and the western tropical Pacific and with a region of divergence over the tropical Atlantic and the eastern Pacific Oceans (Figure 8b). Consequently, the upper-level divergence over the western tropical Pacific and the maritime continent that was characteristic for the 1931 – 1961 period (Figure 8a) has been replaced by an extended upper-level convergence over the maritime continent, the western tropical Pacific, and most of the Indian Ocean, in agreement with the findings of Tokenaga et al (2012). In summary, there is an obvious difference in the Indo-Pacific zonal atmospheric circulation anomalies that can influence the winter Dahlak coral $\delta^{18}\text{O}$ variability during the periods prior and after the 1960's shift. The atmospheric anomaly pattern during the period 1962 – 1992 may be a direct response to the warming trend documented over the Indo-Pacific region since the last 50 years and a corresponding slow down of the Walker Circulation. Similar results, implying a weakening of the Walker

Circulation as a response to a warmer climate, have been also reported by Zhang and Song (2006).

[29] Based on the results shown in this study we propose a two-folded possible physical mechanism for the observed changes in the coral $\delta^{18}\text{O}$ record, ENSO and EAWM:

1) A **tropical connection** (1931 – 1961): La Niña (El Niño) conditions → Cold (warm) tropical Pacific → strong (weak) East Asian Winter Monsoon (**the ENSO dependent mode**) → cold (warm) Indian Ocean → advection of cold (warm) and less saline (saline) waters from the northern Indian Ocean and cold (warm) and dry (wet) air from the Arabian Peninsula into the Southern Red Sea → positive (negative) coral $\delta^{18}\text{O}$. This is a straightforward relationship between the coral record and ENSO, but is valid just for the period 1931 – 1961.

2) An **extratropical connection** (1962 – 1992): a) Indian Ocean warming → weakening of the Walker Circulation → strong convection in the Indian Ocean → ENSO influence over the Indian Ocean and the surrounding areas is reduced → ENSO signal in coral $\delta^{18}\text{O}$ is reduced; and b) weak EAWM (**the mode independent of ENSO**) → weak Siberian High, which in turn allows perturbations from the North Atlantic and the Mediterranean Sea to penetrate as far as western Eurasia → a steep gradient in the Z850 field over the Red Sea → advection of cooler air from the Mediterranean, and continental North Africa and Arabia towards the southern Red Sea. The combined effects of a) and b) control coral $\delta^{18}\text{O}$ during this period: weaker advection of the cooler air masses results in negative coral $\delta^{18}\text{O}$ anomalies at Dahlak, stronger advection results in positive coral $\delta^{18}\text{O}$ anomalies at Dahlak.

5. Conclusions

[30] Our results provide a new perspective on the Dahlak coral $\delta^{18}\text{O}$ record, which reflects temperature and salinity variations in the surface waters of the southern Red Sea, by extending the study of Klein et al. (1997). Klein et al. (1997) have discussed a relation of the winter coral $\delta^{18}\text{O}$ record with the NE monsoon and ENSO, but we show that winter coral $\delta^{18}\text{O}$ variability is linked to SST variability in the Indo – Pacific region via complex atmospheric circulation patterns and two different modes of the EAWM. Furthermore, we find that ENSO dominates the interannual variability of the winter coral $\delta^{18}\text{O}$ record during the period 1931 – 1961. In contrast, during the period 1962 – 1992, when the relationship between the winter coral $\delta^{18}\text{O}$ record and ENSO almost disappears, a strong relationship with a mode of the EAWM that is independent of ENSO becomes more prominent.

[31] The main conclusions of our study are summarized as follows:

- The most important finding of our study, compared to the original interpretation of the Dahlak coral $\delta^{18}\text{O}$ record by Klein et al (1997), is the connection between the winter coral record and the tropical and extra-tropical atmospheric circulation, via the influence of two distinct modes of EAWM. Moreover, we find a non-stationary behavior in the relationship between the coral record and ENSO and EAWM.
- On interannual timescales the large-scale climatic control on the southern Red Sea surface waters during winter is related to both SST variations in the Indo-Pacific region as well as over the whole Red Sea, and to atmospheric processes over the tropics and the Eurasian continent. These processes are strongly influenced by the recent warming trend observed in the Indo-Pacific Oceans.

➤ The first period of the coral record (1931 – 1961) was found to be influenced by pure ENSO related anomalies and an EAWM mode dependent on ENSO. For this period, coral $\delta^{18}\text{O}$ anomalies are associated with ENSO-related SST anomalies throughout the Indian and Pacific Oceans. The atmospheric circulation for this period favors the advection of waters from the Indian Ocean towards the southern Red Sea. During El Niño events, relatively warm Indian Ocean waters are advected towards the north, and are documented as negative coral $\delta^{18}\text{O}$ anomalies at Dahlak. During La Niña events, relatively cool Indian Ocean waters are advected towards the north, and are documented as positive coral $\delta^{18}\text{O}$ anomalies at Dahlak.

➤ The second period (1962 – 1992) is characterized by completely different climate anomalies. Coral $\delta^{18}\text{O}$ anomalies are associated with an atmospheric circulation that projects onto the features of a winter monsoon mode which is independent of ENSO and which favors the advection of cooler air masses from the North Atlantic, Mediterranean, and continental North Africa and Arabia towards the southern Red Sea. Weaker advection of these air masses results in negative coral $\delta^{18}\text{O}$ anomalies at Dahlak, stronger advection results in positive coral $\delta^{18}\text{O}$ anomalies at Dahlak. Importantly, the cold air advection from the north is characterized by a cyclonic circulation over the eastern Mediterranean, and therefore different to the physical mechanism that controls coral $\delta^{18}\text{O}$ in the northern Red Sea, which is characterized by an anticyclonic circulation over the Mediterranean region (Rimbu et al., 2001).

➤ The change and timing of the atmospheric circulation patterns which exert influence on the Dahlak coral $\delta^{18}\text{O}$ record from the southern Red Sea are similar to the tropical Indian Ocean mode shift described by Nakamura et al. (2009).

[33] Based on this study we argue that the southern Red Sea is a suitable location for high-resolution climate reconstructions from marine archives such as annually banded corals, because it is situated in the transition zone between the influence of tropical and extratropical climate systems. Thus, longer coral records from this region can provide the potential to give insights into tropical-extratropical climate interactions throughout the last centuries. Such studies could elegantly complement ongoing paleoclimatic work on modern and fossil corals in the northern Red Sea (e.g., Felis et al., 2004; Felis and Rimbu, 2010; Al Rousan and Felis, 2013), which is a region that is predominantly influenced by extratropical climate systems (Felis et al., 2000; Rimbu et al., 2001).

Acknowledgments. We thank R. Klein for making the Dahlak coral data available. This work was funded by Deutsche Forschungsgemeinschaft through DFG-Research Center/Cluster of Excellence “The Ocean in the Earth System” at the University of Bremen. We thank the two anonymous reviewers for their constructive comments that significantly improved the manuscript.

References

- Al-Rousan, S. and T. Felis (2013) Long-term variability in the stable carbon isotopic composition of *Porites* corals at the northern Gulf of Aqaba, Red Sea. *Palaeogeogr., Palaeoclimatol., Palaeoecol.*, **381–382**, 1-14.
- Annamalai, H., S-P. Xie, J.P. McCreary, and R. Murtugudde (2005), Impact of Indian Ocean sea surface temperature on developing El Niño, *J Climate*, **18**, 302–319.
- Beck, J.W., R.L. Edwards, E. Ito, F.W. Taylor, J. Recy, F. Rougerie, P. Joannot, and C. Henin, (1992), Sea-surface temperature from coral skeletal strontium/calcium ratios, *Science*, **257**, 644–647.
- Boyle, J. S., and T. J. Chen (1987), Synoptic aspects of the wintertime East Asian monsoon. *Monsoon Meteorology*, C. P. Chang, and K. T. N., Eds., Oxford Univ. Press, 125-160.
- Cadet, D. L. (1985), The Southern Oscillation over the Indian Ocean. *J. Climatol.*, **5**, 189–212.
- Chan, J.C.L. (1985), Tropical cyclone activity in the northwest Pacific in relation to the El Niño/Southern Oscillation phenomenon, *Mon. Wea. Rev.*, **113**, 599–606.
- Chang, C. P., and K. M. Lau (1982), Short-term planetary-scale interactions over the tropics and midlatitudes during northern winter. Part I: Contrasts between active and inactive periods, *Mon. Wea. Rev.*, **110**, 933-946.
- Chang, C., Z. Wang, and H. Hendon (2006), The Asian winter monsoon. *The Asian Monsoon*, B. Wang, Ed., Springer Press, 89-127.
- Charles, C.D., D. Hunter, and R.G. Fairbanks (1997), Interaction between the ENSO and the Asian Monsoon in a coral record of tropical climate, *Science*, **277**, 925-928.
- Charles, C.D., K.M. Cobb, M.D. Moore, and R.G. Fairbanks (2003), Monsoon-tropical ocean interaction in a network of coral records spanning the 20th century, *Mar. Geol.*, **201**, 207-222.
- Cobb, K. M., C. D. Charles, H. Cheng, R. L. Edwards (2003), El Niño/Southern Oscillation and tropical Pacific climate during the last millennium, *Nature*, **424**, 271-276.

- Cole, J. E., R. G. Fairbanks, and G. T. Shen (1993), Recent variability in the Southern Oscillation: Isotopic results from a Tarawa Atoll coral, *Science*, **260**, 1790-1793.
- Cole, J. E., R.B. Dunbar, T.R. McClanahan, and N.A. Muthiga (2000), Tropical Pacific forcing of decadal SST variability in the western Indian Ocean over the past two centuries, *Science*, **287**, 617 – 619.
- Compo, G.P., J.S. Whitaker, and P.D. Sardeshmukh (2006), Feasibility of a 100 year reanalysis using only surface pressure data, *Bull. Amer. Met. Soc.*, **87**, 175-190.
- Compo, G.P., J.S. Whitaker, P.D. Sardeshmukh, N. Matsui, R.J. Allan, X. Yin, B.E. Gleason, R.S. Vose, G. Rutledge, P. Bessemoulin, S. Brönnimann, M. Brunet, R.I. Crouthamel, A.N. Grant, P.Y. Groisman, P.D. Jones, M. Kruk, A.C. Kruger, G.J. Marshall, M. Maugeri, H.Y. Mok, Ø. Nordli, T.F. Ross, R.M. Trigo, X.L. Wang, S.D. Woodruff, and S.J. Worley (2011), The Twentieth Century Reanalysis Project, *Quarterly J. Roy. Meteorol. Soc.*, **137**, 1-28. DOI: 10.1002/qj.776.
- Eshel, G., D.P. Schrag and B.F. Farrell (2000), Troposphere–planetary boundary layer interaction and the evolution of ocean surface density: lessons from Red Sea corals, *Journal of Climate*, **13**, 339–351.
- Felis, T., J. Pätzold, Y. Loya, M. Fine, A.H. Nawar, and G. Wefer (2000), A coral oxygen isotope record from the northern Red Sea documenting NAO, ENSO, and North Pacific teleconnections on Middle East climate Variability since the year 1750, *Paleoceanography*, **15(6)**, 679–694.
- Felis, T., G. Lohmann, H. Kuhnert, S.J. Lorenz, D. Scholz, J. Pätzold, J., S. A. Al-Rousan, and S. M. Al-Moghrabi (2004), Increased seasonality in Middle East temperatures during the last interglacial period, *Nature*, **429**, 164-168.
- Felis, T., and N. Rimbu (2010), Mediterranean climate variability documented in oxygen isotope records from northern Red Sea corals - A review, *Global and Planetary Change*, **71**, 232-241.
- Felis, T., A. Suzuki, H. Kuhnert, N. Rimbu, H. Kawahata (2010), Pacific Decadal Oscillation documented in a coral record of North Pacific winter temperature since 1873, *Geophysical Research Letters*, **37**, L14605, doi:10.1029/2010GL043572.

- Gong, D.-Y., S.-W. Wang, and J.-H. Zhu (2001), East Asian winter monsoon and Arctic Oscillation. *Geophys. Res. Lett.*, **28**, 2073–2076, doi:10.1029/2000GL012311.
- Grinsted, A., J.C. Moore, and S. Jevrejeva (2004), Application of the cross wavelet transform and wavelet coherence to geophysical time series, *Nonlinear Processes in Geophysics*, **11**, 561–566.
- Gong, D.Y., Y. Gao, D. Guo, R. Mao, J. Yang, M. Hu, and M. Gao (2013), Interannual linkage between Arctic/North Atlantic Oscillation and tropical Indian Ocean precipitation during boreal winter, *Climate Dynamics*, doi:10.1007/s00382-013-1681-4
- Harris, I., P.D. Jones, T.J. Osborn, and D.H. Lister (2013), Updated high-resolution grids of monthly climatic observations. In press *Int. J. Climatol.* doi: 10.1002/joc.3711
- Hui, G. (2007), Comparison of East Asian winter monsoon indices, *Adv. Geosci.*, **10**, 31-37, doi:10.5194/adgeo-10-31-2007.
- Klein, R., A.W. Tudhope, C.P. Chilcott, J. Pätzold, Z. Abdulkarim, M. Fine, A.E. Fallick and Y. Loya (1997), Evaluating southern Red Sea corals as a proxy record for the Asian monsoon, *Earth and Planetary Science Letters*, **148**, 381-394.
- Klein, S.A., B.J. Soden, and N-C. Lau (1999), Remote sea surface temperature variations during ENSO: Evidence for a tropical atmospheric bridge, *J. Climate*, **12**, 917–932
- Krishnamurthy, V., and B.P. Kirtman (2003), Variability of the Indian Ocean: Relation to Monsoon and ENSO, *Quart. J. Roy. Met. Soc.*, **129**, 1623-1646.
- Kug, J.S., and I.S. Kang (2006), Interactive feedback between ENSO and the Indian Ocean, *J. Climate*, **19**, 1784-1801.
- Lau, N.-C., and M.J. Nath (2003), Atmosphere–Ocean Variations in the Indo-Pacific Sector during ENSO Episodes. *J. Climate*, **16**, 3–20.
- Lau, N.-C., and M.J. Nath (2000), Impact of ENSO on the variability of the Asian–Australian monsoons as simulated in GCM experiments, *J. Climate*, **13**, 4287–4309.
- Li, F., and H. Wang (2012) Predictability of the East Asian winter monsoon interannual variability as indicated by the DEMETER CGCMS, *Adv. Atmos. Sci.*, **29**, 441-454.
- Linsley, B.K., G.M. Wellington, and D. P. Schrag (2000), Decadal sea surface temperature variability in the subtropical South Pacific from 1726 to 1997 A.D., *Science*, **290**, 1145-1148.

- Marengo, J. (1992), Interannual variability of surface climate in the Amazon basin, *Int. J. Climatol.*, **12**, 853–863.
- Nakamura, N., H. Kayanne, H. Iijima, T.R. McClanahan, S.K. Behera, and T. Yamagata (2009), Mode shift in the Indian Ocean climate under global warming stress, *Geophys. Res. Lett.*, **36**, L23708, doi:10.1029/2009GL040590
- Panagiotopoulos, F., M. Shahgedanova, A. Hannachi, and D.B. Stephenson (2005), Observed trends and teleconnections of the Siberian High: A recently declining center of action. *J. Climate*, **18**, 1411–1422.
- Papadopoulos, V.P., Y. Abualnaja, S.A. Josey, A. Bower, D.E. Raitsos, H. Kontoyiannis, and I. Hoteit (2013), Atmospheric forcing of the winter air–sea heat fluxes over the Northern Red Sea, *J. Climate*, **26**, 1685–1701.
- Pfeiffer, M., O. Timm, W.-Chr. Dullo, and D. Garbe-Schönberg (2006), Paired coral Sr/Ca and $\delta^{18}\text{O}$ records from the Chagos Archipelago: Late twentieth century warming affects rainfall variability in the tropical Indian Ocean, *Geology*, **34**(12), 1069–1072. doi: 10.1130/G23162A.1.
- Pfeiffer, M., and W.-Chr. Dullo (2006), Monsoon-induced cooling of the western equatorial Indian Ocean as recorded in coral oxygen isotope records from the Seychelles covering the period of 1840 to 1994 A.D., *Quaternary Science Reviews*, **25**, 993–1009, doi: 10.1016/j.quascirev.2005.11.005.
- Power, S., T. Casey, C. Folland, A. Colman, and V. Mehta (1999), Inter-decadal modulation of the impact of ENSO on Australia, *Clim. Dyn.*, **15**(5), 319–324.
- Rayner, N.A., D.E. Parker, E.B. Horton, C.K. Folland, L.V. Alexander, D.P. Rowell, E.C. Kent, and A. Kaplan (2003), Global analyses of sea surface temperature, sea ice, and night marine air temperature since the late nineteenth century, *J. Geophys. Res.*, **108**, No. D14, 4407, doi: 10.1029/2002JD002670
- Rimbu, N., G. Lohmann, T. Felis, and J. Pätzold (2001), Arctic Oscillation signature in a Red Sea coral, *Geophys. Res. Lett.*, **28**, 2959–2962.
- Rimbu, N., G. Lohmann, T. Felis, and J. Pätzold (2003), Shift in ENSO teleconnections recorded by a northern Red Sea coral, *J. Climate*, **16**, 1414–1422.

- Ronchail J., G. Cochonneau, M. Molinier, J.L. Guyot, A.G. de Miranda Chaves, V. Guimarães, and E. de Oliveira (2002), Interannual rainfall variability in the Amazon basin and sea-surface temperatures in the equatorial Pacific and tropical Atlantic Oceans, *Int J Climatol*, **22**, 1663–1686.
- Saji, N.H., and T. Yamagata (2003), Possible impacts of Indian Ocean Dipole Mode events on global climate, *Climate Research*, **25** (2), 151–169.
- von Storch H., and F. Zwiers (1999), *Statistical Analysis in Climate Research*. Cambridge University Press, 494 pp.
- Timm, O., M. Pfeiffer, and W.-Chr. Dullo (2005), Nonstationary ENSO-precipitation teleconnection over the equatorial Indian Ocean documented in a coral from the Chagos Archipelago, *Geophys. Res. Lett.*, **32**, L02701, doi: 10.1029/2004GL02173.
- Tokinaga H., S. P. Xie, C. Deser, Y. Kosaka, and Y. M. Okumura (2012), Slowdown of the Walker circulation driven by tropical Indo-Pacific warming, *Nature*, **491**:7424, 439-443.
- Torrence, C., and G. P. Compo (1998), A practical guide to wavelet analysis. *Bull. Amer. Meteor. Soc.*, **79**, 61–78.
- Trenberth K.E., and J.W. Hurrell (1994), Decadal atmosphere-ocean variations in the Pacific. *Clim. Dyn.*, **9**, 303–319.
- Whitaker, J.S., G.P. Compo, X. Wei, and T.M. Hamill (2004), Reanalysis without radiosondes using ensemble data assimilation, *Mon. Wea. Rev.*, **132**, 1190-1200.
- Wang, B., Ed., 2006, *The Asian Monsoon*. Springer Praxis, 799pp.
- Watanabe, M., and F.-F. Jin (2002), Role of Indian Ocean warming in the development of Philippine Sea anticyclone during ENSO, *Geophys. Res. Lett.*, **29**(10), doi:10.1029/2001GL014318,.
- Wei, K., W. Chen, and W. Zhou (2011), Changes in the East Asian cloud season since 2000, *Adv. Atmos. Sci.*, **28**, 69-79.
- Wu, B., and J. Wang (2002), Winter Arctic Oscillation, Siberian high and East Asian winter monsoon. *Geophys. Res. Lett.*, **29**, 1897, doi:10.1029/2002GL015373
- Wu, B-Y., R. Zhang, and R. D'Arrigo (2006), Distinct modes of the East Asian winter monsoon, *Mon. Wea. Rev.*, **134**, 2165–2179.

Zhang, R., A. Sumi, and M. Kimoto (1996), Impact of El Niño on the East Asian monsoon: A diagnostic study of the '86/87 and '91/92 events. *J. Meteorol. Soc. Jpn.*, **74**, 49-62.

Zhang, Y., J.M. Wallace, and D.S. Battisti (1997), ENSO-like interdecadal variability: 1900-93, *J Climate*, **10**, 1004–1020.

Zhang, M., and H. Song (2006), Evidence of deceleration of atmospheric vertical overturning circulation over the tropical Pacific, *Geophys. Res. Lett.*, **33**, L12701, doi:10.1029/2006GL025942.

Zhong, A., H.H. Hendon, and O. Alves (2005), Indian Ocean Variability and Its Association with ENSO in a Global Coupled Model, *J. Climate*, **18**, 3634–3649.

Zhou, W., X. Wang, T. J. Zhou, C. Li, and J.C.L. Chan (2007), Interdecadal variability of the relationship between the East Asian winter monsoon and ENSO, *Meteorol. Atmos. Phys.*, **98**, 283-293.

Zhou, L.T. (2011), Impact of East Asian winter monsoon on rainfall over southeastern China and its dynamical process, *Int. J. Climatol.*, **31**, 677–86.

Zinke, J., M. Pfeiffer, O. Timm, W.-Chr. Dullo, and G. R. Davies (2005), Atmosphere-ocean dynamics in the western Indian Ocean recorded in corals, *Philos. Trans. R. Soc., Ser. A*, **363**, 121–142.

Figure captions.

Figure 1. Location map of the Red Sea and the northern Indian Ocean.

Solid head arrows indicate the direction of 850mb winds during the winter NE monsoon season and line contours represent the mean NDJF air temperature at 1000mb.

Units: air temperature ($^{\circ}\text{C}$) and wind speed (m/s)

Figure 2. Normalized time series of Dahlak winter (JF) coral $\delta^{18}\text{O}$ record (black) and NDJF Niño 3.4 index (green). The red lines indicates the time when the correlation shifts from $r = -0.63$ to almost zero.

Figure 3. a) The 21-yr running correlation coefficients between the time series of the winter (JF) Dahlak coral $\delta^{18}\text{O}$ record and the winter (NDJF) Niño 3.4 index (black), winter EAWM (red) and winter EAWM_{en} (blue) for the period 1931–1992;

b) The 21-yr running correlation coefficients between the time series of the winter (JF) Dahlak coral $\delta^{18}\text{O}$ record and the winter Siberian High index (blue) and EAWM_{res} (red) for the period 1931–1992. Running correlation coefficients are plotted at the midpoint of each window; for example, the value at 1941 stands for the correlation during the period 1931–1952.

c) The continuous wavelet power spectrum for the JF coral $\delta^{18}\text{O}$ record (upper panel) and NDJF Niño 3.4 index (lower panel). Black contours bind regions that are significant against a red noise null hypothesis.

d) Squared wavelet coherence between the JF coral $\delta^{18}\text{O}$ record and NDJF Niño 3.4 index. Arrows indicate the phase of the coherence, where right is in phase and left is in out-of-phase.

Figure 4. a) Correlation map between winter (JF) Dahlak coral $\delta^{18}\text{O}$ record and NDJF global SST for the period 1931 – 1961;

b) Correlation map between winter (NDJF) EAWM_{en} index and NDJF global SST for the period 1931 – 1961;

c) Correlation map between winter (JF) Dahlak coral $\delta^{18}\text{O}$ record and NDJF global SST for the period 1962 – 1992;

d) Correlation map between winter (NDJF) EAWM_{res} index and NDJF global SST for the period 1962 – 1992. For a better comparison with Figure 4c we have multiplied the EAWM_{res} index with (-1).

Figure 5. a) Geopotential Height at 850 mb (Z850 – shaded areas) and 850mb Wind vectors (arrows) composite map (difference between averaged maps for which the winter (JF) Dahlak

coral $\delta^{18}\text{O}$ record was higher (lower) than 0.75 (-0.75) standard deviation) for the period 1931 – 1961.

b) As in **a)** but for EAWM_{en} index;

c) As in **a)** but with a focus over the Indian Ocean and Red Sea

(the black arrow indicates the wind direction)

Units: wind (m/s).

Figure 6. a) Geopotential Height at 850 mb (Z_{850} – shaded areas) and 850mb Wind vectors (arrows) composite map (difference between averaged maps for which the winter (JF) Dahlak coral $\delta^{18}\text{O}$ record was higher (lower) than 0.75 (-0.75) standard deviation) for the period 1962 – 1992.

b) As in **a)** but for EAWM_{res} index. The winter EAWM_{res} index has been multiplied with (-1) for a better comparison with Figure 6a.

c) As in **a)** but with a focus over the Indian Ocean and Red Sea

(the black arrow indicates the wind direction).

Units: wind (m/s).

Figure 7. a) Correlation maps between winter (JF) Dahlak coral $\delta^{18}\text{O}$ record and NDJF TT over land for the period 1931 – 1961.

b) As in **a)**, but for the period 1962 – 1992.

Figure 8. a) 200 mb velocity potential (shaded) and divergent wind (wind bars) composite map (difference between the averaged maps for which the normalized winter (JF) Dahlak coral $\delta^{18}\text{O}$ record was higher (lower) than 0.75 (-0.75) standard deviation) for the period 1931 – 1961.

b) As in **a)**, but for the period 1962 – 1992.

Units are: $10^6 \text{ m}^2/\text{s}$ for the velocity potential and m/s for the divergent wind.

Mean NDJF Air Temperature (1000mb)
Mean NDJF Wind (850mb)

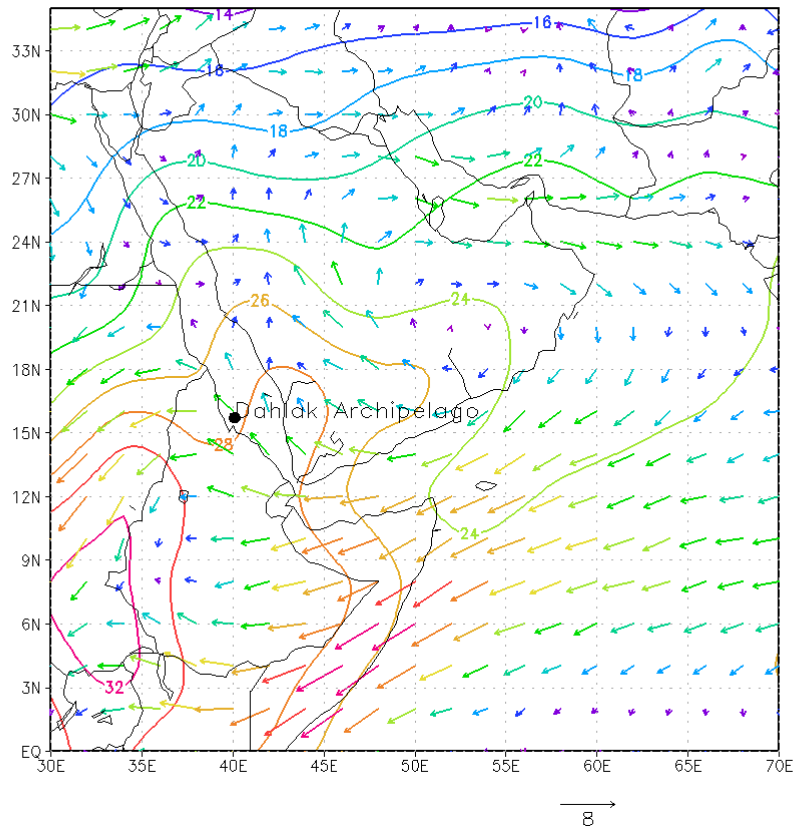


Figure 1. Location map of the Red Sea and the northern Indian Ocean.

Solid head arrows indicate the direction of 850mb winds during the winter NE monsoon season and line contours represent the mean NDJF air temperature at 1000mb.

Units: air temperature (°C) and wind speed (m/s)

Accepted

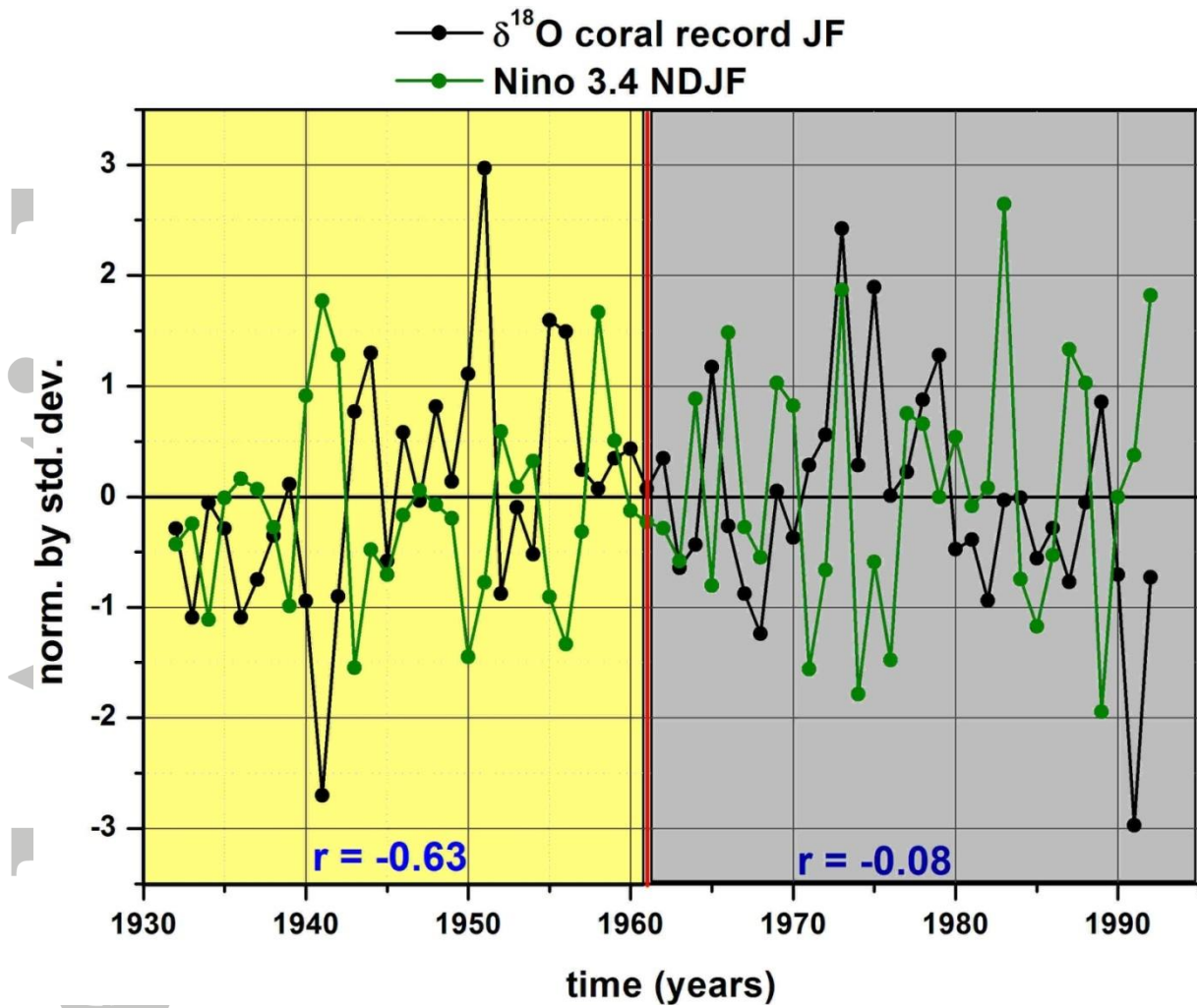
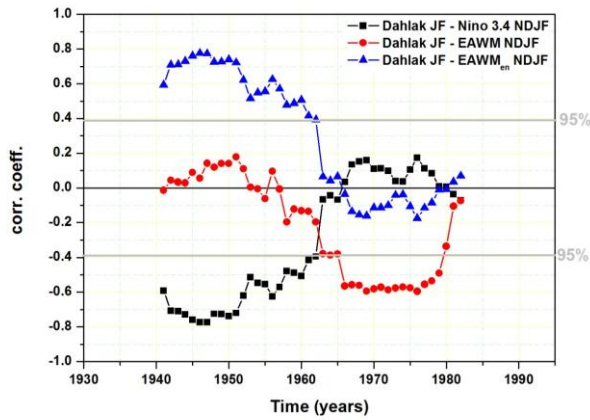


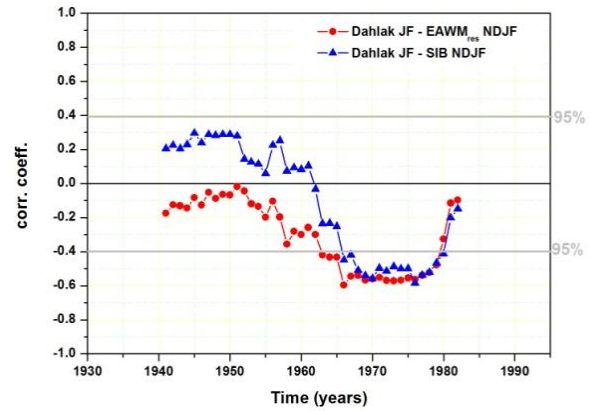
Figure 2. Normalized time series of Dahlak winter (JF) coral $\delta^{18}\text{O}$ record (black) and NDJF Niño 3.4 index (green). The red lines indicates the time when the correlation shifts from $r = -0.63$ to almost zero.

Accepted

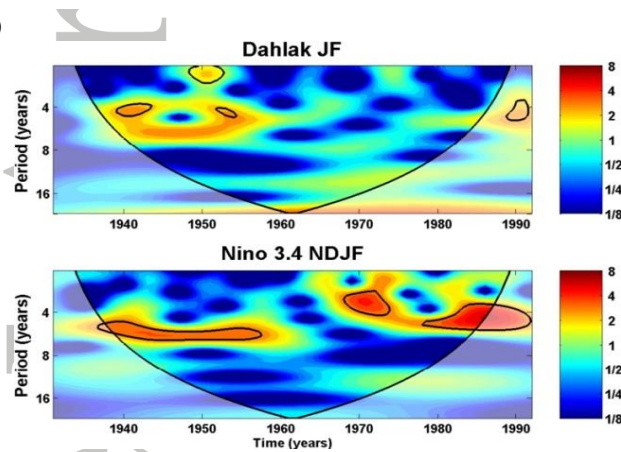
a)



b)



c)



d)

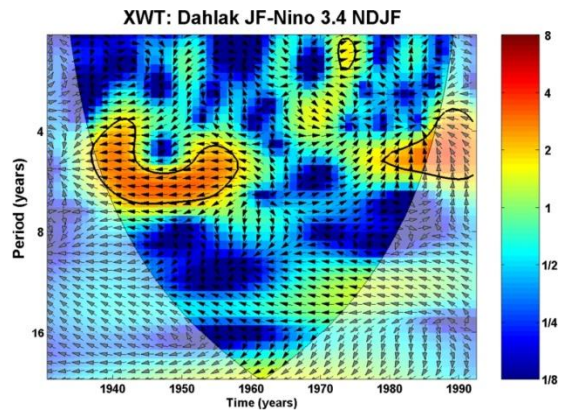


Figure 3. a) The 21-yr running correlation coefficients between the time series of the winter (JF) Dahlak coral $\delta^{18}\text{O}$ record and the winter (NDJF) Niño 3.4 index (black), winter EAWM (red) and winter EAWM_{en} (blue) for the period 1931–1992;

b) The 21-yr running correlation coefficients between the time series of the winter (JF) Dahlak coral $\delta^{18}\text{O}$ record and the winter Siberian High index (blue) and EAWM_{res} (red) for the period 1931–1992. Running correlation coefficients are plotted at the midpoint of each window; for example, the value at 1941 stands for the correlation during the period 1931–1952.

c) The continuous wavelet power spectrum for the JF coral $\delta^{18}\text{O}$ record (upper panel) and NDJF Niño 3.4 index (lower panel). Black contours bind regions that are significant against a red noise null hypothesis.

d) Squared wavelet coherence between the JF coral $\delta^{18}\text{O}$ record and NDJF Niño 3.4 index. Arrows indicate the phase of the coherence, where right is in-phase and left is in out-of-phase.

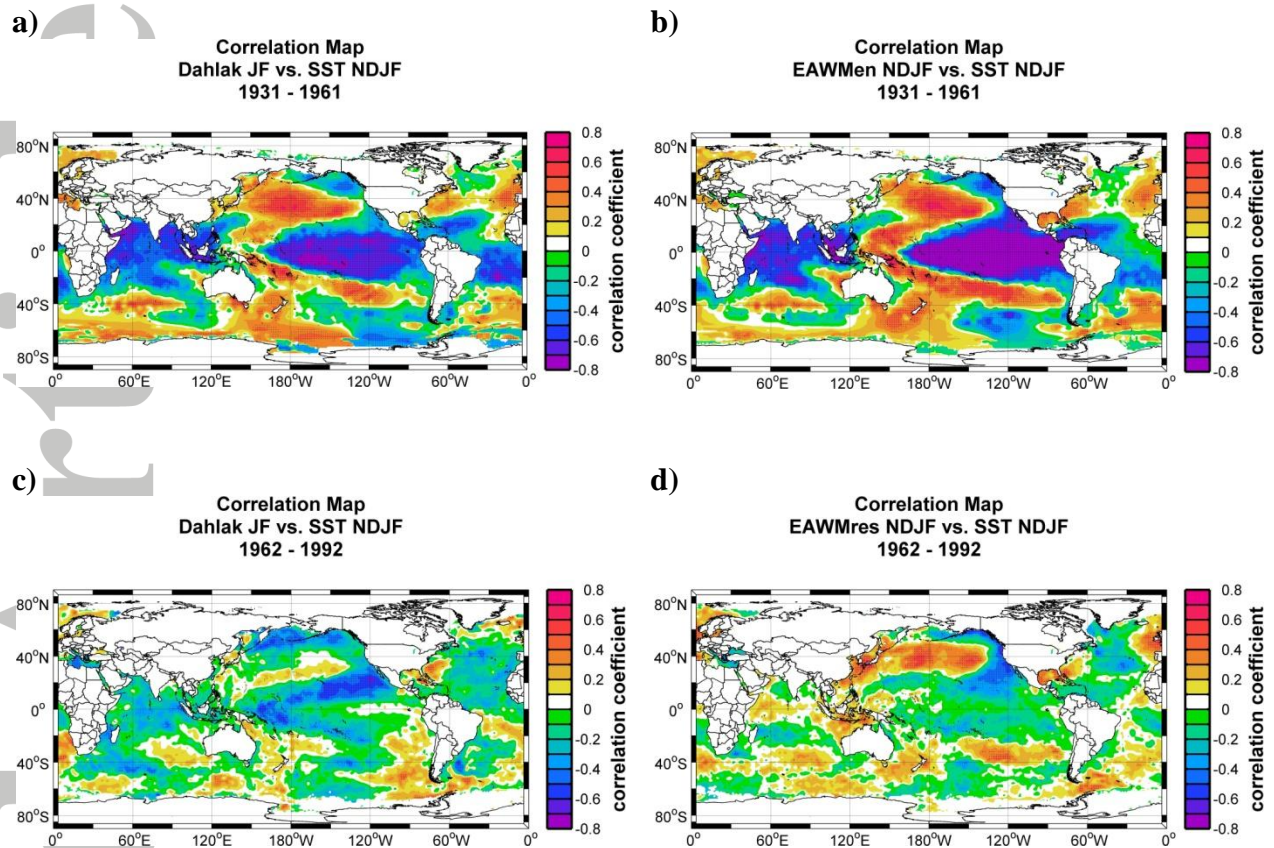


Figure 4. a) Correlation map between winter (JF) Dahlak coral $\delta^{18}\text{O}$ record and NDJF global SST for the period 1931 – 1961;
 b) Correlation map between winter (NDJF) EAWM_{en} index and NDJF global SST for the period 1931 – 1961;
 c) Correlation map between winter (JF) Dahlak coral $\delta^{18}\text{O}$ record and NDJF global SST for the period 1962 – 1992;
 d) Correlation map between winter (NDJF) EAWM_{res} index and NDJF global SST for the period 1962 – 1992.

For a better comparison with Figure 4c we have multiplied the EAWM_{res} index with (-1).

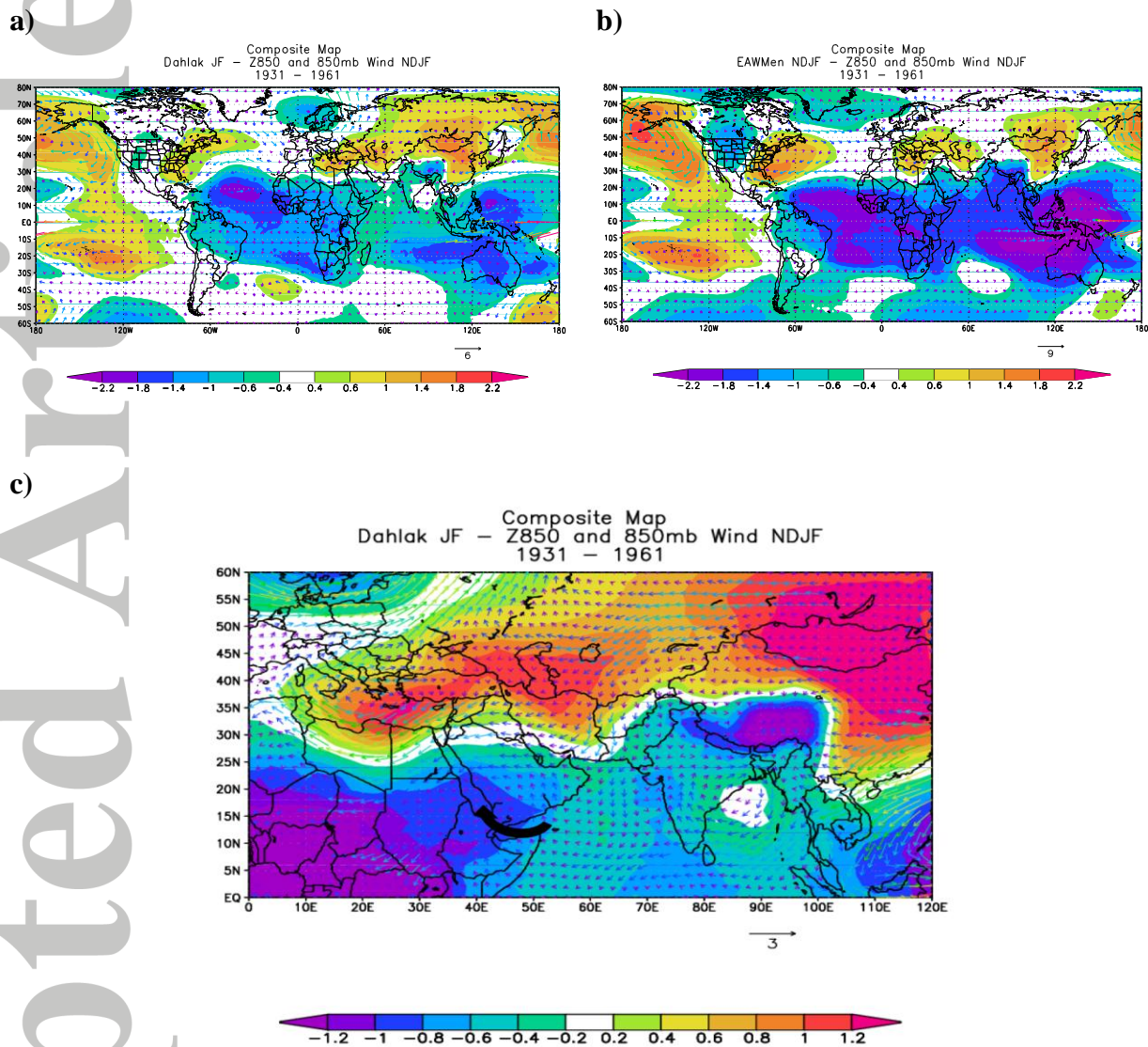


Figure 5. a) Geopotential Height at 850 mb (Z850 – shaded areas) and 850mb Wind vectors (arrows) composite map (difference between averaged maps for which the winter (JF) Dahlak coral $\delta^{18}\text{O}$ record was higher (lower) than 0.75 (-0.75) standard deviation) for the period 1931 – 1961.

b) As in **a)**, but for EAWM_{en} index;

c) As in **a)** but with a focus over the Indian Ocean and Red Sea (the black arrow indicates the wind direction)

Units: wind (m/s).

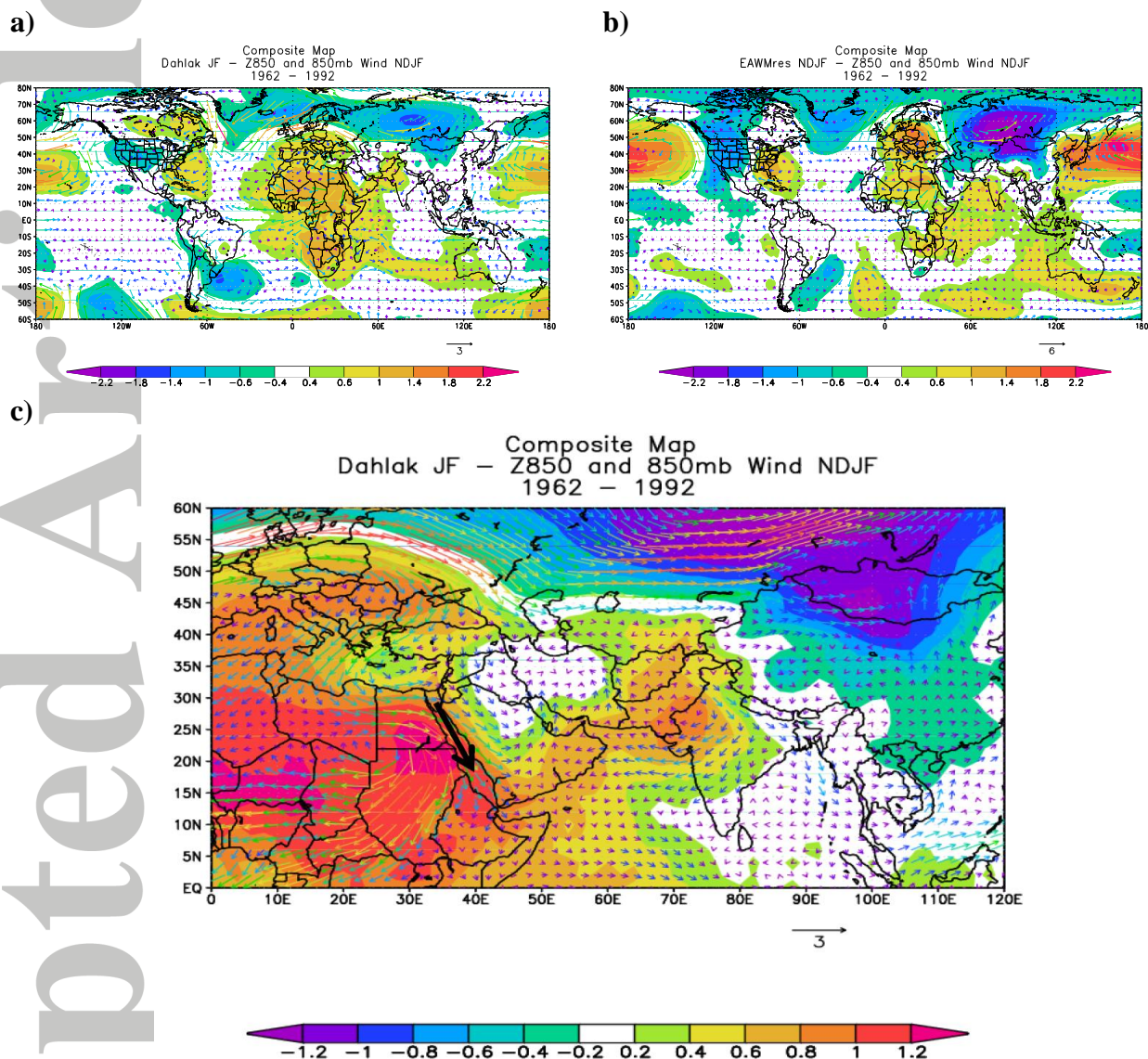


Figure 6. a) Geopotential Height at 850 mb (Z850 – shaded areas) and 850mb Wind vectors (arrows) composite map (difference between averaged maps for which the winter (JF) Dahlak coral $\delta^{18}\text{O}$ record was higher (lower) than 0.75 (-0.75) standard deviation) for the period 1962 – 1992.

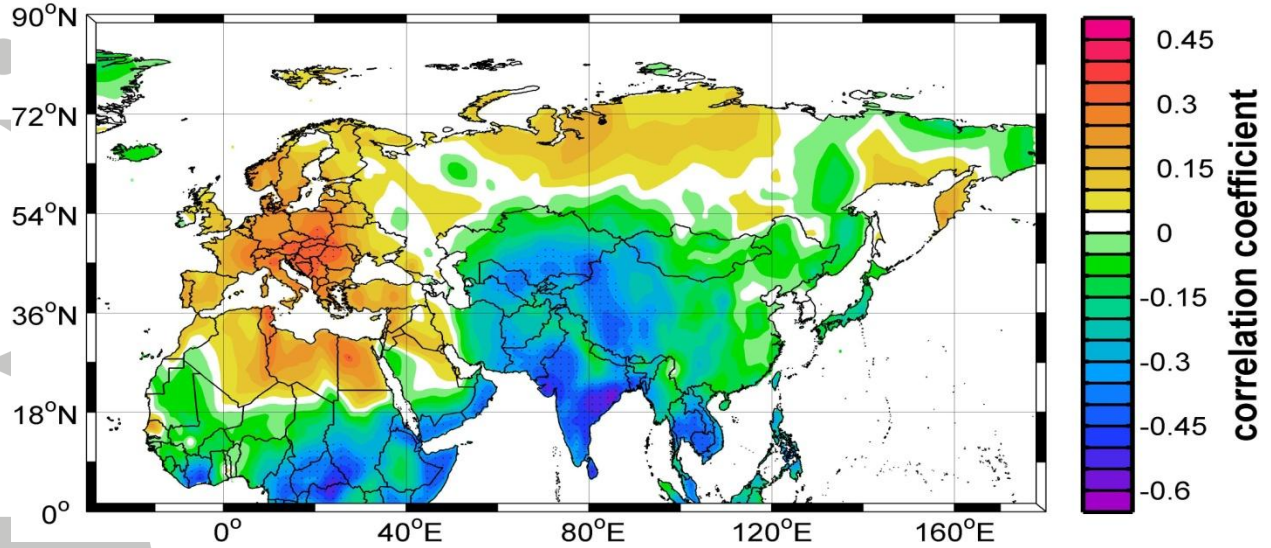
b) As in **a)**, but for EAWM_{res} index. The winter EAWM_{res} index has been multiplied with (-1) for a better comparison with Figure 6a.

c) As in **a)** but with a focus over the Indian Ocean and Red Sea (the black arrow indicates the wind direction).

Units: wind (m/s).

a)

**Correlation Map
Dahlak JF vs. TT NDJF
1931 - 1961**



b)

**Correlation Map
Dahlak JF vs. TT NDJF
1962 - 1992**

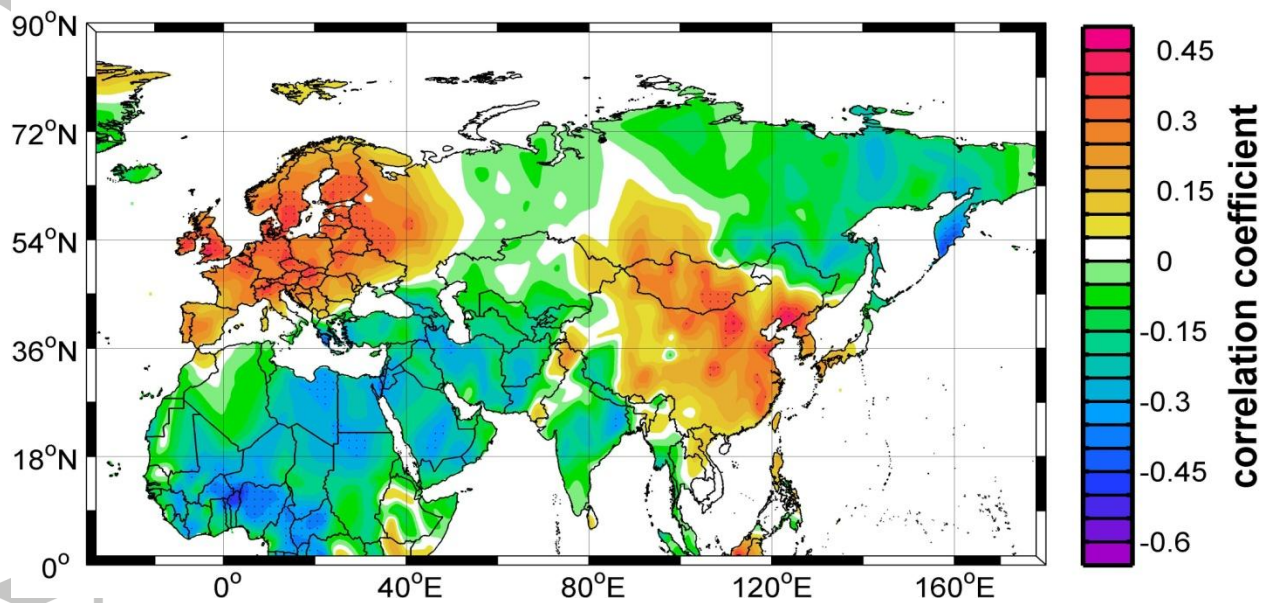
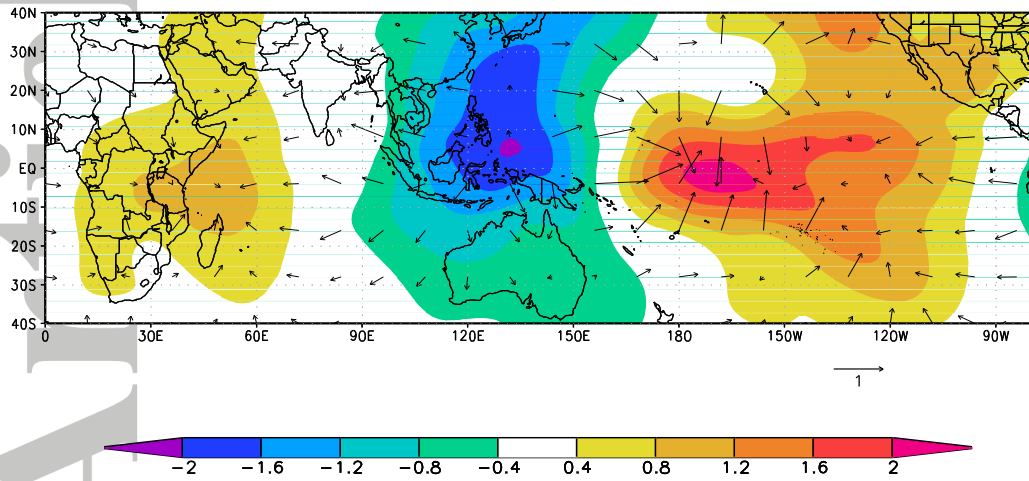


Figure 7. a) Correlation maps between winter (JF) Dahlak coral $\delta^{18}\text{O}$ record and NDJF TT over land for the period 1931 – 1961.
b) As in a), but for the period 1962 – 1992.

a)

Composite Map
Dahlak JF - 200mb Velocity Potential & Divergent Wind NDJF
1931 - 1961



b)

Composite Map
Dahlak JF - 200mb Velocity Potential & Divergent Wind NDJF
1962 - 1992

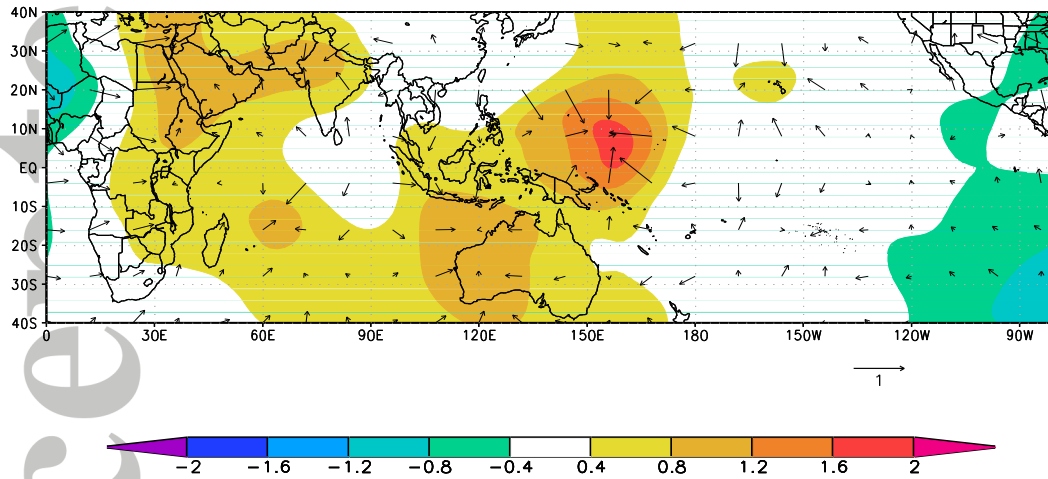


Figure 8. a) 200 mb velocity potential (shaded) and divergent wind (wind bars) composite map (difference between the averaged maps for which the normalized winter (JF) Dahlak coral $\delta^{18}\text{O}$ record was higher (lower) than 0.75 (-0.75) standard deviation) for the period 1931 - 1961.

b) As in a), but for the period 1962 - 1992.

Units are: $10^6 \text{ m}^2/\text{s}$ for the velocity potential and m/s for the divergent wind.